Article

Cells as Active Particles in Asymmetric Potentials: Motility under External Gradients

Jordi Comelles,[1,2,3] David Caballero,[1,2] Raphaël Voituriez,[7,8] Verónica Hortigüela,[4,5] Viktoria Wollrab,[1,2] Amélie Luise Godeau,[1,2] Josep Samitier,[3,5,6] Elena Martínez,[4,5,6] and Daniel Riveline[1,2,*]

[1]Laboratory of Cell Physics ISIS/IGBMC, CNRS UMR 7006 and University of Strasbourg, Strasbourg, France; [2]Development and Stem Cells Program, IGBMC, CNRS UMR 7104, INSERM (U964) and University of Strasbourg, Illkirch, France; [3]Nanobioengineering Group, Institute for Bioengineering of Catalonia (IBEC), Barcelona, Spain; [4]Biomimetic Systems for Cell Engineering, Institute for Bioengineering of Catalonia (IBEC), Barcelona, Spain; [5]Centro de Investigación Biomédica en Red en Bioingeniería, Biomateriales y Nanomedicina, Zaragoza, Spain; [6]Department of Electronics, University of Barcelona, Barcelona, Spain; [7]Laboratoire de Physique Théorique de la Matière Condensée, CNRS UMR 7600, Université Pierre et Marie Curie, Paris, France; and [8]Laboratoire Jean Perrin, CNRS FRE 3231, Université Pierre et Marie Curie, Paris, France

ABSTRACT Cell migration is a crucial event during development and in disease. Mechanical constraints and chemical gradients can contribute to the establishment of cell direction, but their respective roles remain poorly understood. Using a microfabricated topographical ratchet, we show that the nucleus dictates the direction of cell movement through mechanical guidance by its environment. We demonstrate that this direction can be tuned by combining the topographical ratchet with a biochemical gradient of fibronectin adhesion. We report competition and cooperation between the two external cues. We also quantitatively compare the measurements associated with the trajectory of a model that treats cells as fluctuating particles trapped in a periodic asymmetric potential. We show that the cell nucleus contributes to the strength of the trap, whereas cell protrusions guided by the adhesive gradients add a constant tunable bias to the direction of cell motion.

INTRODUCTION

Cell migration plays key roles in a variety of physiological processes, ranging from development (1) to pathological processes, such as cancer (2). Cells can migrate directionally, following a persistent trajectory along the same direction of an axis (3). Such cell behavior drives the tissue rearrangements that shape organs in embryos (4). Directed cell movement is also associated with cancer metastasis (5). In adults, dendritic cells migrate directionally from the interstitial space into the lymphatic vessels, thereby participating to the onset of the immune response (6). Altogether directional motility is a generic feature of living cells.

Mechanisms behind cell migration have been studied in several in vitro assays. Topographical features in the shape of grooves have been shown to guide nondirectional cell migration along the main axis of grooves in both directions, in a mechanism known as contact guidance (7–11). In these situations, cells align according to features much smaller than the size of the cell itself by attaching mainly to the top of the topographical structures (7,10,11). Furthermore, several studies report directional cell motion in vitro by imposing asymmetric cues to the cells. In addition to asymmetric one-dimensional paths, both chemical (12–15) and topographical (16–18), adhesive (19) and stiffness gradients (20) also direct cell migration. On these substrates, cell motion is often understood to be directional—with a persistent trajectory along the same direction of an axis— because the cell symmetry is broken by the external cues. For example, it was shown that there is greater activity of cell protrusions at the front of the cell than at its tail (21). However, when directional cell motion is achieved in these experiments, the cellular organelle setting directions is often not known. In addition, the prediction of cell direction as a function of the cues and geometries imposed is not straightforward. Finally, the quantitative comparison of cell motion with a model is often lacking. In light of these observations, new approaches that link the biology of the cell to the physics of living matter are required.

Here, we report a new, to our knowledge, assay in which we tested the effects of external cues on single fibroblast cell directed motion. The cellular mechanisms at play were identified and motions were quantified and compared with a model. Specifically, using substrates with ratchet-shaped topographical patterns, we show that the nucleus dictates the directions of cell movement through mechanical guidance. A ratchet stands as a paradigm for studying symmetry breaking (22–24). Directionality can be tuned when topography is combined with a superimposed fibronectin adhesion gradient. We observed competition and cooperation between the effects of the two external cues depending on their relative orientations. We adapt a theory of fluctuating particles trapped in a periodic asymmetric potential, introduced by Prost et al. (23,24), to model cell behavior.

Submitted December 16, 2013, and accepted for publication August 1, 2014.

*Correspondence: riveline@unistra.fr

Editor: Ewa Paluch.

0006-3495/14/10/1513/10 $2.00

http://dx.doi.org/10.1016/j.bpj.2014.08.001

We found that the nucleus contributes to the strength of the topographical trap, whereas cell protrusions guided by the adhesive gradients add a constant tunable bias to the motion.

MATERIALS AND METHODS

Substrate fabrication

The ratchet-shaped topographical pattern was made on Poly(methyl methacrylate) (PMMA) substrates. Topographical motifs were produced by standard photolithography and nanoimprint lithography (25,26). Briefly, first a SU-8-2015 (MicroChem Corp, Newton MA) positive master with microstructures was obtained by standard photolithography, the resulting mold was replicated on a poly(ethylene naphthalate) (Goodfellow, Huntingdon,UK) sheet (125 μm thick) by nanoembosing to obtain a negative replica. This secondary mold was then used to transfer the structures to the PMMA surface. The design of the structures is an array of triangles of 100 μm in length, 22 μm in width, and 1 μm in height, forming a ratchet-like topographic pattern (see Fig. S1, *b* and *c* in the Supporting Material) over a total area 25 mm in length and 1 mm in width. The dimensions of the triangles were chosen on the basis of the mean size of a NIH 3T3 cell (see Fig. S2). The triangle area (1100 μm^2) corresponds to the mean half-area of a NIH 3T3 fibroblast spread on a homogeneous fibronectin layer (100 ng.cm^{-2}).

The imprinted structures were characterized by means of scanning electron microscopy (Strata DB235, FEI, The Netherlands) and white light interferometry (Wyko NT110, Veeco Metrology, USA).

Gradient formation

The procedure used for gradient formation is described elsewhere (26). Briefly, a fibronectin gradient was generated on a previously hydrolyzed PMMA surface (either flat or structured) by means of a polydimethylsiloxane Y-shaped microfluidic channel (Sylgard 184 Silicon Elastomer, Dow Corning, Wiesbaden, Germany), which allowed the control of protein concentration across the channel. The flow rates and exposure times were set to obtain a linear protein gradient (26). A 1:39 mixture of fluorescently labeled and unlabeled fibronectin was used (20 μg ml^{-1} solution of fibronectin in phosphate buffered saline, rhodamine fibronectin from bovine plasma (Cytoskeleton, Denver, CO) and fibronectin from bovine plasma (Sigma-Aldrich, Saint-Quentin Fallavier, France). After gradient formation, the PMMA substrate was detached from the microfluidic channel. The remaining regions on the surface were saturated with a poly(L-lysine)-graft-poly(ethylene glycol) co-polymer (PLL-g-PEG) molecule (PLL (20)-g [3.5]-PEG (2), Susos, Dübendorf, Switzerland) to prevent adsorption of molecules from the cell culture medium and to reduce nonspecific cell adhesion. The shape of the fibronectin gradient was checked before each experiment by fluorescence microscopy (Fig. S1, *d* and *f*), with a CKX41 microscope (Olympus) using the Wasabi acquisition system (Hamamatsu) and a cooled couple-charge device camera (Hamamatsu). Homogenous fibronectin surfaces (either flat or structured) were achieved using the same microfluidic system. For this purpose, only the fibronectin solution was flowed through the channel and with the conditions used for high-density fibronectin regions of the gradient (100 ng.cm^{-2}) (26).

Cell migration experiments

The NIH 3T3 mouse embryonic fibroblast cell line (ATCC) was grown for 3 days at 37°C in Dulbecco's modified Eagle medium (D-MEM) (Invitrogen, Cergy Pontoise, France) supplemented with 10% bovine calf serum (BCS) (Invitrogen, Cergy Pontoise, France). Before the experiments, cells were trypsinized and replated on the PMMA surface in D-MEM with 10% BCS. After 20 min, unattached cells were removed by washing with fresh medium. Finally, for time-lapse experiments the medium was replaced by L-15 (Leibovitz's L-15 medium, Invitrogen, Cergy Pontoise, France) with 1% BCS serum.

Cells were observed under a CKX41 Olympus microscope using a 4× phase-contrast objective for around 48 h at 37°C. Images were acquired every 5 min. A 20× phase-contrast objective was used for high-magnification observations.

Cell migration experiments-side view

NIH 3T3 fibroblasts were plated on a glass coverslip and incubated for 1 h in the incubator. The coverslip was held by two binder clips. Clips allowed to place the coverslip vertically oriented under the microscope. Cells were visualized on the side in L-15 medium with 10% BCS.

Transfections and staining

NIH 3T3 fibroblasts were transfected with zyxin-red fluorescent protein (RFP) and nonmuscle myosin heavy chain II - Green Fluorescent Protein (called here myosin-GFP). Transient transfection was performed 1 day before experiment using Lipofectamine 2000 (Life Technologies), according to the manufacturer's instructions. Cells were fixed using 3% PFA (Sigma-Aldrich), and nuclei were stained with DAPI.

Cell trajectory evaluation

The centroid trajectories of cells were tracked using the manual tracking plug-in in ImageJ (http://rsb.info.nih.gov/ij, NIH). Data analysis was performed using a custom-made code in MATLAB (The MathWorks, Natick, MAA). Cell positions were characterized by a vector $\mathbf{r}(t)$, with t denoting time and $\mathbf{r}$ position in space (bold letter refers to a vector). Every recorded cell position during the time-lapse experiment was defined as $\mathbf{r}_i = \mathbf{r}(t_i)$, where $t_i = i\Delta t$ are the times of recording and Δt denotes the duration of time-lapses. The vector difference between two positions is then defined as $\Delta\mathbf{r}_{ij} = \mathbf{r}_i - \mathbf{r}_j$ and its length $||r_i||$ and angle with the x axis of the frame of reference of the laboratory $\cos(\theta_{ij}) = \Delta\mathbf{r}_{ij} \cdot \mathbf{i} / ||\Delta\mathbf{r}_{ij}||$, can be computed. To describe cell trajectories, a displacement vector ($\boldsymbol{\delta}$) and an angular distribution $\{\theta_{ij}\}$ were used. The displacement vector is calculated as the vector difference between the initial ($t = t_0$) and final point ($t = t_f$), $\boldsymbol{\delta} = \mathbf{r}(t = t_f) - \mathbf{r}(t = t_0)$. And the angular distribution was obtained from $\cos(\theta_{ij})$, being $i\Delta t$ - $j\Delta t = 60$ min (see Fig. S3). This duration was longer than the 5 min time-lapse acquisition, but it captured displacements within the resolution of our experiment. >30 cells from at least 3 independent experiments were evaluated for each configuration.

When modeling cell trajectories, we focus our study on persistent movement (27), i.e., migrating without stopping. We define a cell pause when its centroid is still for 30 min within our spatial resolution; a new persistent trajectory then starts. Our measurement of steps in lattice units evaluates persistent trajectories and conditional probabilities with this rule.

RESULTS

Directing cell migration with a ratchet-like topography

We developed a topographical ratchet-like surface that was combined with a fibronectin coating of spatially controlled density (Fig. 1 and Fig. S1). We first tracked cells moving on a ratchet-like surface covered with a homogeneous layer of fibronectin (see Fig. 1 *c*, *left* and Movie S1). These trajectories were compared with those of cells moving on a flat surface covered with the same density of fibronectin

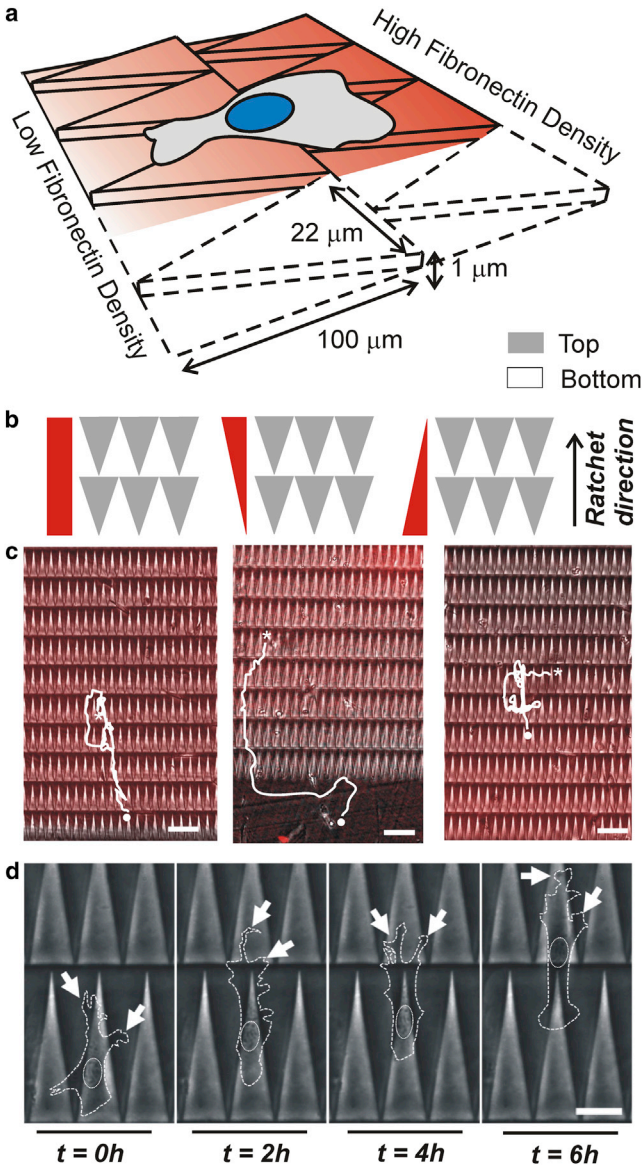

FIGURE 1 The motility assay. (*a*) Schematics of the experimental setup. Cells moved on topographical ratchets coated with fibronectin. The lattice unit of triangular shape measured 22 μm in width, 100 μm in length, and 1 μm in height. (*b*) Experimental conditions: topographical ratchet with homogeneous fibronectin coating; fibronectin gradient in the direction of the ratchet (indicated by an *arrow*); and fibronectin gradient against the direction of the ratchet. (*c*) Cells moving on topographical ratchets combined with homogeneous fibronectin coating, gradient up and gradient down, respectively. In white, cell trajectory, the red signal shows fibronectin, and • and * the start and end of the trajectories, respectively. Scale bar 100 μm. (*d*) Specific time sequence of a cell moving over topographical motifs. In this case, the cell migrates directionally along the bottom triangles. White arrows highlight cell protrusions. Scale bar 20 μm. To see this figure in color, go online.

(Fig. 2 *b*, configuration (i) and (ii)). Cells moved freely on the flat surface, leading to isotropically distributed tracks (Fig. 2 *b* configuration (i)). In contrast, ratchet-like patterns oriented the direction of cell migration along the y axis (Fig. 2 *b* configuration (ii)). We confirmed the isotropic behavior of cells on flat surfaces in the angular distribution plot of cell directions every 60 min (see Fig. 2 *c* configuration (i) *red curve*), where no peak was observed (see Fig. S4 *a*). Similarly, we observed an angular distribution asymmetry for cells moving on the topographical pattern (see Fig. 2 *c* configuration (ii)) with a primary peak ($\theta_1 = 86 \pm 20$ (^{o})) and a secondary peak ($\theta_2 = 264 \pm 29$ (^{o})), along the ratchet directions (Fig. S4 *b*). We next plotted the mean displacement vector, i.e., the averaged sum of vectors between the start and end points of each trajectory (see Fig. 2 *c* configuration (i) and (ii) *green arrow* and Fig. S5). The vectors indicated that net motion was isotropic and random on flat surfaces, whereas it was rectified toward the positive y axis on the ratchet pattern. Previous gradient-free strategies relied on cell confinement, either chemical (12–15) or physical (16–18). However, here we show that cells on an asymmetric topographical pattern, with no restriction in adhesiveness or physical confinement, moved in the direction imposed by the features of the ratchet itself.

Cell nucleus sets the direction

To further explore this symmetry breaking in cell migration, we analyzed cell behavior at a higher magnification (Movie S2 and Movie S3). When the cell nucleus interacted with the side walls of the triangular structures, the nucleus trajectory was rectified, which led to a change in the whole cell trajectory. A typical example is shown in Fig. 3 *a*: when the cell was moving from a top triangle (*dark*) to a bottom triangle (*bright*), the nucleus experienced two rectifications of trajectory (Fig. 3 *a*, *left* and Movie S2). On the other hand, a cell first performing a lateral movement was then directed toward the vertex of the triangle (Fig. 3 *a*, *right* and Movie S3). The correlation of the nucleus trajectory and the topography walls points to the occurrence of a contact interaction, which would explain the asymmetry observed in cell migration. This evidence is supported by inhomogeneity of the density and shape of nuclei outlines in Fig. 3 *a*. This finding indicates a mechanical interaction between the topographical walls and the cell nucleus.

We next obtained quantitative insight into this nucleus—wall mechanical interaction. We measured the fraction of time that the nucleus of migrating cells spent at the top and bottom of the structures, as well as the percentage of nuclei placed at the top and bottom of the motifs on fixed samples. In the former case, the nucleus was located 63 $\pm$ 7% of the time on the bottom triangles (Fig. 3 *b*). This tendency was maintained in fixed samples (69 $\pm$ 3%) (Fig. 3 *c*). Moreover, a noneven distribution of cell nucleus position was observed in the ratchet framework. We superimposed the nucleus position of >400 cells on a single ratchet unit and generated the corresponding color map (Fig. 3 *d*). Most of the nuclei were distributed in the widest region of a bottom triangle. This finding suggests

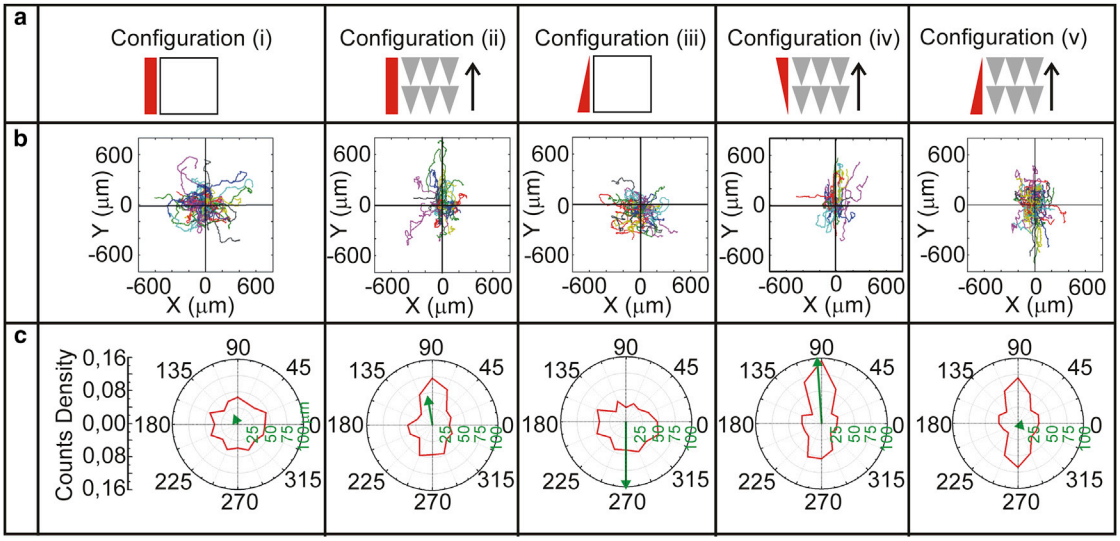

FIGURE 2 The cell trajectories. (*a*) Experimental configurations: (i) flat surface coated with a homogeneous layer of fibronectin, (ii) topographical ratchet coated with a homogenous layer of fibronectin, (iii) flat surface coated with a fibronectin gradient, (iv) topographical ratchet coated with a fibronectin gradient up, and (v) with a fibronectin gradient down. (*b*) Merge of cell trajectories for each configuration during the same total duration (48 h). All tracks start at the origin of the graph. $N_i = 6$, $n_i = 70$, $N_{ii} = 4$, $n_{ii} = 30$, $N_{iii} = 3$, $n_{iii} = 40$, $N_{iv} = 3$, $n_{iv} = 33$, $N_v = 3$, $n_v = 62$ (N number of biological repeats and n number of cells analyzed). (*c*) Angular distribution and displacement vectors. Red curve represents the histogram of the migration angle (every 60 min, $n_i = 2253$ steps, $n_{ii} = 953$ steps, $n_{iii} = 1275$ steps, $n_{iv} = 990$ steps, $n_v = 2060$ steps) and the green vector the mean displacement vector (the sum of the vectors between the start and end points of each cell, averaged by the number of cells $N_i = 6$, $n_i = 70$, $N_{ii} = 4$, $n_{ii} = 30$, $N_{iii} = 3$, $n_{iii} = 40$, $N_{iv} = 3$, $n_{iv} = 33$, $N_v = 3$, $n_v = 62$). The green scale corresponds to the length of the vector in μm. To see this figure in color, go online.

that the topographical ratchet pattern traps the nucleus in an analogous manner as an energy potential well would trap a particle.

To further study the nature of this interaction, we analyzed whether the nucleus shape and orientation were altered by the topographical patterns (see Fig. S6 and Fig. S7). For this purpose, we fit the nucleus edge to an ellipse and measured the major axis a, the minor axis b, and the angle $\boldsymbol{\alpha}$ between the ellipse and the laboratory framework axis (Fig. 3 *e*). On fixed samples, cell nuclei located at the top of the triangles were more elongated than those at the bottom (Fig. S6 *e* and Fig. S6 *f*). Moreover, nuclei showed a random angular distribution on the top triangles (Fig. 3 *f*). In contrast, a peak distributed around 90° appeared when nuclei were at the bottom. To obtain further insight into the dynamical interaction between the nucleus and the topographical landscape, change in nucleus orientation was studied in time-lapse experiments. The following results show that the nucleus is interacting with the topographical ratchet: i), as it can be seen in the examples shown in Fig. S7, *a* and *b*, nucleus orientation changed when moving from top to bottom; ii), nucleus tended to realign parallel to the direction set by the topographical walls; iii), nuclei were randomly oriented when moving on top of triangles, and they oriented around 90° when moving in bottom triangles (Fig. S7 *c*), as observed in fixed samples (Fig. 3 *f*); iv), whenever nuclei interacted with the topographical walls, they reoriented accordingly to the directions set by the walls (Fig. S7 *d*). These observations suggest that the orientation and the mechanical deformation of the nucleus depend on its interaction and its position on the ratchet framework (see also (28) for a related discussion based on a different setup). This feature is essential in the model proposed below.

To analyze the role of the cytoskeleton in cell behavior on topographical ratchets, we transfected 3T3 fibroblasts with myosin-GFP and zyxin-RFP (see Movie S4). No striking correlation was observed between protrusions and the topographical pattern. Cells spread on both top and bottom triangles, and there was no preferential orientation observed in cell shape (see Fig. S8 *a*). Moreover, peripheral focal contacts could be observed on top triangles, bottom triangles and, eventually at the topographical walls (Fig. S8 *b*). In contrast, we observed the appearance of focal contacts correlating with the topographical walls close to the nucleus (see Movie S5 and Fig. S8 *c*). When the nucleus contacted a wall, focal contacts nucleated at the location of the neighboring wall. These focal contacts then elongated and the nucleus passed over the structure. When the nucleus had passed the structure, the zyxin signal decreased and eventually disappeared. These observations support the idea of a mechanical interaction between the topographical pattern and the nucleus.

Tuning ratchet efficiency by using adhesive gradients

We addressed whether, in addition to the role of the nucleus setting cell direction based on the ratchet topography, we

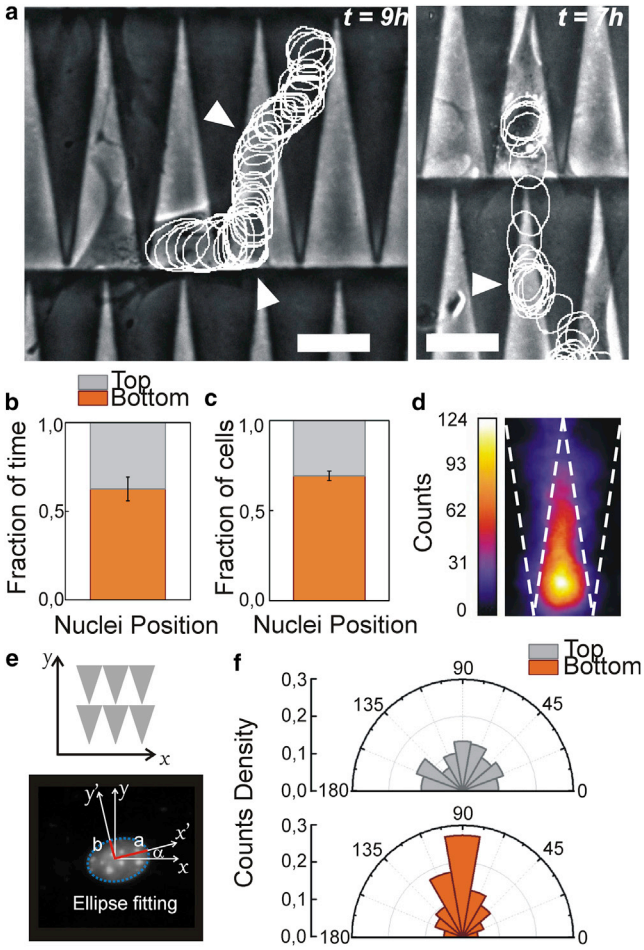

FIGURE 3 The role of the nucleus. (*a*) Image of a cell migrating in topographical ratchets coated with a homogenous layer of fibronectin. White circles outline the positions of the nuclei at various time points (every 15 min). White arrows show changes in directions after nucleus-wall contacts. Scale bar 20 μm, *t*: time spent to perform this particular movement. (*b*) Fraction of time that nuclei spent on top triangles and on bottom triangles during the motion. (total time $>$ 8 h, $N = 4$ experiments, $n = 11$ cells, mean values $\pm$ standard errors). (*c*) Fraction of cells in which the nucleus was positioned on top triangles and on bottom triangles on fixed samples ($N = 3$ experiments, $n = 654$ cells, mean values $\pm$ standard errors). (*d*) Color map of the mean nucleus position on a lattice unit. Bottom triangles pointing up and top triangles pointing down ($N = 3$ experiments, $n > 400$ cells). (*e*) Scheme for the ellipse fit of nuclei. Major (*a*) and minor (*b*) axes of the ellipse were obtained using ImageJ, and the relative angle between the ellipse and the ratchet framework was measured. (*f*) Plot of the nuclei orientation, histogram of the angles α for nuclei at the top (*gray*) and at the bottom (*orange*) of the structures ($N = 3$ experiments, $n = 654$ cells). To see this figure in color, go online.

could externally induce cell polarization and asymmetry in lamellipodia activity, thus tuning ratchet efficiency. Fig. 2 *b* configuration (iii) shows the cell trajectories moving on a fibronectin gradient on a flat surface (gradient slope 0,1 $(\text{ng}\cdot\text{cm}^{-2})\cdot\mu\text{m}^{-1}$). Compared to configuration (i), cell trajectories were not restricted to the *x* or *y* axis, but were biased toward regions of high fibronectin density. The gradient directed cell motion from weakly adhering regions to strongly adhering ones (19,29). This result was further confirmed by both the angular distribution and the mean displacement vector (Fig. 2 *c*, configuration (iii) and Fig. S4 *c* and Fig. S5).

We next combined the fibronectin gradient with the topographical ratchet (change of fibronectin density within 1 triangle is 10 $\text{ng}\cdot\text{cm}^{-2}$). We first tested the situation where the gradient and the ratchet rectified cell motion to the same direction (Fig. 1 *c*, *middle* and Movie S6). Similar to the ratchet case, cell trajectories were distributed along the *y* axis and biased toward positive *y* values (Fig. 2 *b* configuration (iv)). However, compared to the ratchet alone, the angular distribution in this configuration was more biased to the 90° direction (primary peak $\theta_1 = 92 \pm 18$ (°) and secondary peak $\theta_2 = 262 \pm 22$ (°)) (see Fig. 2 *c* configuration (iv) and Fig. S4 *d* and Fig. S5), suggesting an increase in the rectification efficiency. This result was further confirmed by the mean displacement vector (Fig. 2 *c* configuration (iv)).

We finally set the gradient and the ratchet in opposite directions (Fig. 1 *c*, *right* and Movie S7). In this case, the tracks were again aligned with the *y* axis. The angular distribution showed two main directions with similar probability: primary peak $\theta_1 = 92 \pm 18$ (°) and secondary peak $\theta_2 = 269 \pm 19$ (°) (Fig. 2 *c* configuration (v) and Fig. S4 *e* and Fig. S5). This finding indicates that there was still a preferential cell movement along the *y* axis, but there was no net bias in cell motion rectification. Configuration (v) showed a mean displacement vector similar to that of (i) (Fig. 2 *c*). The ratchet efficiency was reduced and cell motion was no longer rectified. Thus, the ratchet and gradient competed.

Modeling cell trajectories

To analyze the degree of bias efficiency, we discretized cell motion in lattice units (l.u.) (1 triangle = 1 l.u.). We then quantified the number of steps that cells took in each direction and classified them into three types: 1), positive (+), when a cell moved from one row of triangles to the next in the ratchet direction; 2), minus (−), when the motion was in the opposite direction; and 3), lateral (0), when cells persistently moved laterally within one row of triangles, either right or left by symmetry (Fig. 4 *a*). We then obtained the probability of each type of step (Π_+, Π_-, Π_0), which allowed comparison between configurations (Fig. 4 *a* – *solid arrows* – and *b*). The bias (Fig. 4 *c*) associated with the ratchet (configuration (ii)) was $\Pi_+/\Pi_- = 1.42 \pm 0.07$. Bias increased to 1.64 ± 0.15 when the ratchet and the gradient were cooperating (configuration (iv)). Finally, the competition (configuration (v)) between the ratchet and the gradient led to a bias of $\Pi_+/\Pi_- = 1.04 \pm 0.26$, in agreement with the tendency observed for the displacement vectors. Therefore our results show that the bias in cell migration produced by the ratchet could be increased/decreased by superimposing an adhesive gradient in the same or opposite directions.

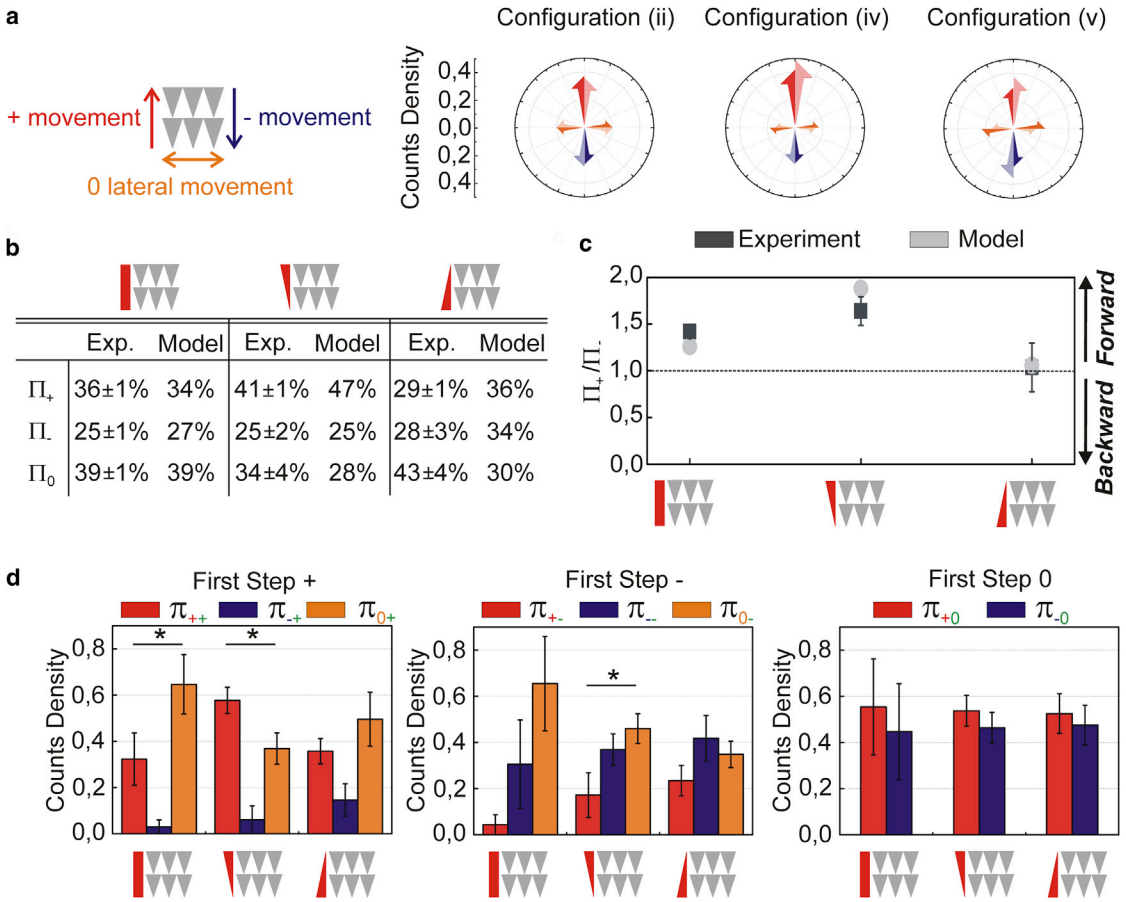

FIGURE 4 Comparisons between the experiments and the model. (*a*) Classification of the cell movements used to quantify the ratchet bias. Mean probabilities to move toward a given direction in configurations (ii), (iv), and (v) respectively. (*Solid half arrows* and percentages correspond to experimental values, *patterned half arrows* correspond to the values predicted by the model). (*b*) Comparison of the experimental and theoretical values of the moving probabilities (Π_i) for each configuration (Mean values ± standards error, $N_{ii} = 4$ experiments, $n_{ii} = 214$ movements, $N_{iv} = 3$ experiments, $n_{iv} = 147$ movements, $N_v = 3$ experiments, $n_v = 367$ movements). (*c*) Comparison of the experimental and theoretical biases Π_+/Π_- for the configurations (ii), (iv), and (v). (*d*) Probabilities of the eight possible transitions in each of the three experimental configurations (mean values ± standards error, First step + $N_{ii} = 4$ experiments, $n_{ii} = 59$ transitions, $N_{iv} = 3$ experiments, $n_{iv} = 37$ transitions, $N_v = 3$ experiments, $n_v = 63$ transitions, First step 0 $N_{ii} = 4$ experiments, $n_{ii} = 38$ transitions, $N_{iv} = 3$ experiments, $n_{iv} = 23$ transitions, $N_v = 3$ experiments, $n_v = 66$ transitions, First step - $N_{ii} = 4$ experiments, $n_{ii} = 39$ transitions, $N_{iv} = 3$ experiments, $n_{iv} = 29$ transitions, $N_v = 3$ experiments, $n_v = 66$ transitions). (*) statistically significant differences $p < 0.05$. To see this figure in color, go online.

To further analyze cell trajectories and assess the importance of potential memory effects, we experimentally measured the conditional probability of performing a +, −, or 0 step, which depends on the previous move performed in the absence of pauses, i.e., during a persistent trajectory (Fig. 4 *d* and Fig. S9; see Methods). More precisely, these transition probabilities π_{ji}, where $i,j = +, -, 0$, are defined as the probability that a cell performs a step in the direction j, knowing that the previous step was performed in direction i. Normalization then imposes $\pi_{+i} + \pi_{-i} + \pi_{0i} = 1$. The π_{ji} encodes two effects responsible for the direction of migration: the local asymmetry of both the topographic landscape and adhesion profile, and the direction of the previous move, which here encodes the polarization state of the cell. We have $\pi_{++} \neq \pi_{+-}$ (see Fig. 4 *d*): this clearly shows that the memory of the previous move influences the direction of the next one. This first move is likely to polarize cells (Fig. 1 *d*) and to affect the internal organization of organelles. We hereafter assume that the dependence on the previous only (1 step memory) is sufficient to describe cell trajectories, and that the dependence on earlier moves can be neglected. The direct analysis of such longer range memory would require longer persistent trajectories with no pauses and is not statistically significant with our data sets (4 ± 1 steps per persistent movement—including 0 steps—on average). Under this minimal hypothesis, cell motion can be modeled as a persistent random walk, an approach that has proved useful in the context of cell trajectory analysis (30,31).

This model allowed us to relate the observed large-scale properties in the trajectories to elementary transition probabilities π_{ji} introduced previously. We derive in the

Supporting Material the expressions of the main characteristics of the trajectories as a function of π_{ji} only: the stationary probabilities Π_+, Π_-, Π_0, which provide the probabilities that a step is performed in direction $+$, $-$, 0 in a steady state, regardless of the nature of the previous step; and the persistence lengths, which give the mean number of consecutive steps performed in a given direction. With the experimentally measured values of π_{ji}, we computed the theoretical values of Π_+, Π_-, Π_0, and the persistence lengths. As seen in Fig. 4 *a* (*patterned arrows*) and Fig. 4 b, the predicted values of Π_+, Π_-, Π_0, and the biases (Fig. 4 *c*) are in good agreement with the experimental observations, as well as persistence lengths (see Fig. S10). The observed discrepancy in configuration (v) results from steps 0 where cells can be in any polarity state or even unpolarized, which is not taken into account explicitly in the model; this is especially relevant in this configuration where two external cues are competing. This finding indicates that cell trajectories are well described by persistent random walks, which constitute a minimal model that takes into account both the cell polarization state (through the memory of the previous step) and external cues that can bias the motion.

Finally, we aimed to link the π_{ji} to the properties of the local environment of the cell, i.e., both topography and adhesion properties. We followed the picture of a particle in a tilted washboard potential, as introduced in Constantini et al. (32). Therefore, the central hypothesis was, as suggested previously, that cell movement is impaired mainly by the nucleus, which must mechanically deform to pass the successive obstacles formed by the topographic landscape (28), as observed in Fig. 3. Here, we assume that the nucleus is confined to the substrate by a normal force (for example the vertical component of the pulling force mediated by stress fibers (33)) (see Fig. 5 *a*). Actually, by imaging cell migration on the side on flat surfaces, we could observe that i), nucleus was occupying a large fraction of cell volume; ii), its height was varying with time and was correlated to the cell spreading; and iii), the nucleus was very close to the surface, suggesting a potential sensitivity to any change in surface profile (see Fig. S6 *a* and Movie S8). Moreover, when observing NIH 3T3 fibroblast transfected with myosin-GFP on flat surfaces, it can be seen that the appearance of prominent stress fibers correlate with an increase of nucleus projected area, suggesting that it is indeed flattening (see Fig. S6 *b*). These observations point to the presence of a normal force confining the nucleus to the surface related to stress fibers, which eventually correlate with the walls of the topographical pattern (Movie S5 and Fig. S8 *c*).

This implies that the cell nucleus effectively moves in an energetic potential $U_E(x,y)$ (Fig. 5 *b*), corresponding to the stored mechanical energy, which we propose is of elastic origin in a first approximation (34). Following the previous observation that the nucleus deformation depends on the

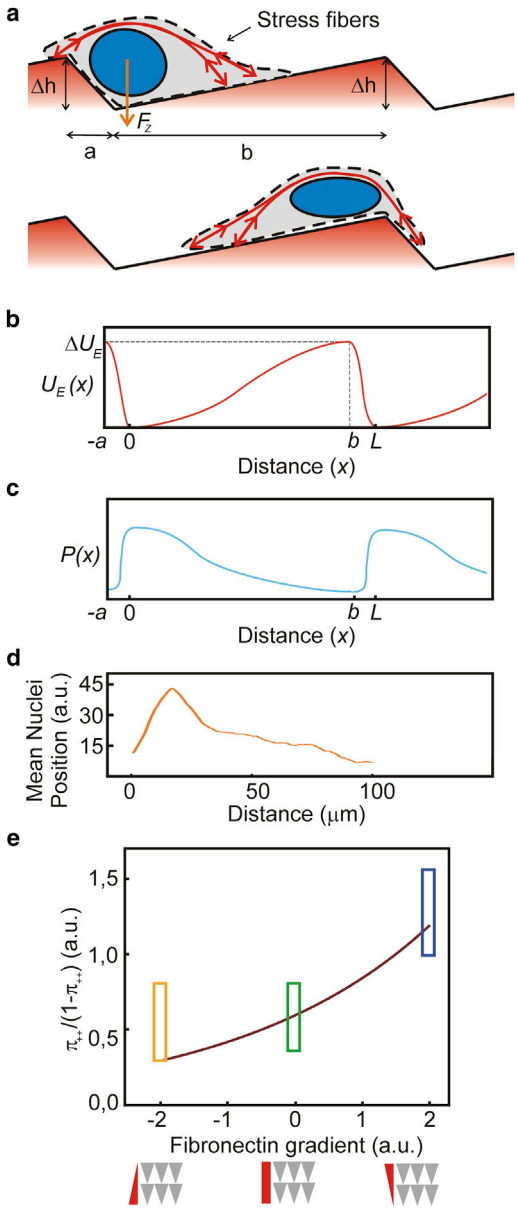

FIGURE 5 Cells as active particles in asymmetric potentials. (*a*) Schematics of a cell in an asymmetric topographical landscape. Cell nucleus experiences a normal compressive force F_z, imposing a mechanical deformation to pass the successive obstacles. (*b*) Energetic potential $U_E(x,y)$. (*c*) Probability distribution $P_n(x)$ of the nucleus position at steady state. (*d*) Mean nuclei position, obtained experimentally from Fig. 3 *d*. (*e*) Dependence of π_{ij} on the fibronectin gradient. The brown curve represents the evolution of the ratio $\pi_{++}/(1-\pi_{++})$ for different fibronectin gradient slopes. The yellow, green, and blue boxes are the measured values for this ratio in the three experimental configurations (v, ii, and iv), respectively. To see this figure in color, go online.

position in the ratchet, we assume that the energetic potential $U_E(x,y)$, which we do not aim to determine explicitly here, is directly correlated to the height profile $h(x,y)$ of the landscape (see Fig. S1). The resulting probability distribution $P_n(x)$ of the nucleus position in a steady state can readily be deduced and peaks at the minima of h (see

Fig. 5 *c*). This description is supported by the experimental observation that the stationary distribution of nuclei positions peaked at the location of local minima of $h(x,y)$ (Fig. 3 *d* and Fig. 5 *d*). The period of the ratchet in the y direction is denoted by $L = a + b$. The profile $U_E(x,y)$ is assumed to successively decrease with a slope $\Delta U/a = F_-$ over a distance a, and then increase with slope $\Delta U/b = F_+$ over a distance b, with $(a < b)$ (see Fig. 5 *c*). This shows that at least a force F_+ (*resp.* F_-) must be exerted along the $+y$ (*resp.* $-y$) direction to induce a step in the $+y$ (*resp.* $-y$) direction; the condition $F_+ < F_-$ then clearly indicates that the direction $+$ is favored.

To estimate the propulsion force experienced by a cell, we consider a minimal model of cell locomotion and assume that the cell propulsion force is mediated by individual protrusions. Following ideas developed in (27), we introduce the mean number (per unit time) of protrusions stabilized in direction i, z_{ij}, where $i = +,-$. Following the finding that the direction of motion depends on the direction of the previous move, z_{ij} depend on the direction of the previous move. Note that here we focus on the ratchet direction $+/-$, but similar definitions would hold for the direction 0. We define the probability $p(n_+)$ that n_+ protrusions are stabilized in the $+$ direction (and similarly in the $-$ direction). We assume that it follows a Poisson distribution of mean $z_+ \tau_0$, where τ_0 is the mean duration time of an elementary step and the dependence on the previous move is omitted for clarity. We then introduce the asymmetry of stabilized protrusions $\Delta = n_+ - n_-$. This quantity is shown in the Supporting Material to be distributed according to

$$P(\Delta) = e^{-(z_+ + z_-)\tau_0} \left(\frac{z_+}{z_-}\right)^{\Delta/2} I_\Delta(2\tau_0\sqrt{z_+ z_-}), \qquad (1)$$

where $I_\Delta(x)$ is the first kind, to our knowledge, of modified Bessel function of Δ-th rank. Assuming that each efficient protrusion transmits a unit force (in the properly normalized unit of force), Eq. 1 gives the probability that a total force Δ is transmitted by protrusions.

Finally, the condition $\Delta \geq F_+$ that motion occurs in the $+$ direction enables an explicit calculation of π_{+i} that reads:

$$\pi_{+i} = e^{-(z_{+i} + z_{-i})\tau_0} \sum\nolimits_{\Delta \geq F_+} \left(\frac{z_{+i}}{z_{-i}}\right)^{\Delta/2} I_\Delta(2\tau_0\sqrt{z_{+i} z_{-i}}). \qquad (2)$$

A similar expression holds for π_{-i}.

These expressions combine in a simple form the effects of the topographic ratchet (through the dependence on F_+), adhesion properties (encoded in z_{ji}), and the polarization state of the cell (encoded in the dependence on the previous move) on cell motion. They allow a semiquantitative discussion of the experiments in configurations (ii), (iv), and (v). In particular, the bias can be quantified here by the ratio π_{+i}/π_{-i}, and was found, as expected, to increase with the ratchet asymmetry b/a and the efficiency of protrusion activity z_{ji}. Assuming that the mean number of effective protrusions is proportional to the local concentration of fibronectin, one can write $z_{+i} = z_{-i} + \alpha\nabla c$. The dependence of π_{ij} on the fibronectin gradient can then be calculated. Fig. 5 *e* shows that this dependence is well captured by the model, which in particular can account for both competition and cooperation effects.

DISCUSSION

We have proven that cell motion can be directed by a topographical asymmetric pattern with no previous confinement of cell movement, either physical or biochemical. We identified the mechanical interaction between the cell nucleus and the topographical walls as a possible mechanism to explain the rectification of cell movement. By combining the topographic ratchet with an adhesive gradient, we tuned its rectification efficiency, thereby suggesting that asymmetries in cell polarization increase or decrease the efficiency of the ratchet depending on their relative orientations.

Previous studies achieved biased cell motion by asymmetric patterns, either chemical (12–15) or physical (13,16–18), that induced cell polarization by means of confining cells and restricting their motion to one-dimensional. Geometrical asymmetries in the pattern design amplified natural differences in lamellipodia activity at the front and the rear of a polarized cell, leading to directed motion (12–15,17,18). Because we used homogeneous fibronectin coatings and topographical patterns smaller than the cell size and of a moderate height (35), we did not restrict cell migration in any direction. Thus, the bias that we observed stems from a different origin.

Recent studies have shown that nucleus trapping caused by spatial constraints of the three-dimensional (3D) environment is a limiting factor for cell migration (36), as cell movement is arrested when the nucleus cannot overcome physical barriers imposed by a 3D collagen network. Similar behavior has been observed for cells migrating in channels (37). Our results are in agreement with this phenomenon, confirming that physical interaction between the nucleus and the environment architecture is a determinant factor in cell migration, even in nonconfined cells. Moreover, we report a role for cell nucleus in setting directionality, where mechanical interaction between the nucleus and the physical constraints is a subtle interplay between nucleus elasticity, topographical landscape, and protrusion activity (36). Furthermore, we noticed the appearance of focal contacts colocalizing with the topographical walls when nucleus contacted the walls of the topographical pattern. This observation could be related to a noneven distribution of forces on the nucleus, thus leading to the nucleus reorientation.

Moreover, we show that the bias in cell migration induced by the nucleus-topography interaction can be tuned by adding an external adhesive gradient. This finding suggests that

both nucleus impairment and traction force, i.e., the adhesion to the fibronectin layer, cooperate or compete in setting cell migration. In other words, we show that when the traction force is in the opposite direction of the topographical ratchet, cells more easily overcome the topographical walls. Similarly, 3D cell migration experiments revealed that integrin-mediated traction force is required to propel the nucleus forward when its movement is impaired by physical constraints (36).

Finally, we successfully captured the essential features of the system by modeling cells as particles in asymmetric potentials. This theoretical model was based on two main experimental observations: i), cell motion within the ratchet depends on the direction of the previous movement, which is a minimal way to encode polarization; and ii), the motion is restricted by the mechanical interaction between the nucleus and the topographical landscape. Interestingly, this analysis, based on a microscopic modeling of motion at the cell scale, showed that long-term cell trajectories are robustly described as simple persistent random walks, in agreement with earlier results (38). This observation contrasts with findings at smaller scales where Lévy walk features have been reported (39). This new approach to cell motility with disentangled contributions is proposed as a generic framework for understanding cell motion in vitro and in vivo.

SUPPORTING MATERIAL

Ten figures, eight movies, and supporting data are available at http://www.biophysj.org/biophysj/supplemental/S0006-3495(14)00805-4.

We thank the members of Riveline's lab for critical discussions. We thank E. Fuchs (Rockefeller University) for the zyxin-RFP construct and E. Paluch (UCL) for the nonmuscle myosin heavy chain II-GFP construct. We acknowledge the Nanotechnology Platform of the IBEC and D. Izquierdo for technical support.

This work was supported by funds from the CNRS (D.R.), the University of Strasbourg (D.R.), the ci-FRC of Strasbourg (D.R.), Fondation Simone et Cino del Duca (J.C., D.R.), the CIBER-BBN initiative (V.H., E.M., J.S.), the "Generalitat de Catalunya" (2009 SGR 505 J.S. and BE fellowship to J.C.), and the "Fundación Botín" (E.M., J.S.). The authors declare no competing financial interests.

SUPPORTING CITATIONS

Reference (40) appears in the Supporting Material.

REFERENCES

1. Bénazéraf, B., P. Francois, …, O. Pourquié. 2010. A random cell motility gradient downstream of FGF controls elongation of an amniote embryo. *Nature.* 466:248–252.
2. Giampieri, S., C. Manning, …, E. Sahai. 2009. Localized and reversible TGFbeta signalling switches breast cancer cells from cohesive to single cell motility. *Nat. Cell Biol.* 11:1287–1296.
3. Petrie, R. J., A. D. Doyle, and K. M. Yamada. 2009. Random versus directionally persistent cell migration. *Nat. Rev. Mol. Cell Biol.* 10:538–549.
4. Lecaudey, V., G. Cakan-Akdogan, …, D. Gilmour. 2008. Dynamic FGF signaling couples morphogenesis and migration in the zebrafish lateral line primordium. *Development.* 135:2695–2705.
5. Calvo, F., N. Ege, …, E. Sahai. 2013. Mechanotransduction and YAP-dependent matrix remodelling is required for the generation and maintenance of cancer-associated fibroblasts. *Nat. Cell Biol.* 15:637–646.
6. Weber, M., R. Hauschild, …, M. Sixt. 2013. Interstitial dendritic cell guidance by haptotactic chemokine gradients. *Science.* 339: 328–332.
7. Teixeira, A. I., G. A. Abrams, …, P. F. Nealey. 2003. Epithelial contact guidance on well-defined micro- and nanostructured substrates. *J. Cell Sci.* 116:1881–1892.
8. Kim, D.-H., C.-H. Seo, …, K.-Y. Suh. 2009. Guided cell migration on microtextured substrates with variable local density and anisotropy. *Adv. Funct. Mater.* 19:1579–1586.
9. Kim, D.-H., K. Han, …, A. Levchenko. 2009. Mechanosensitivity of fibroblast cell shape and movement to anisotropic substratum topography gradients. *Biomaterials.* 30:5433–5444.
10. Kim, H. N., Y. Hong, …, K.-Y. Suh. 2012. Effect of orientation and density of nanotopography in dermal wound healing. *Biomaterials.* 33:8782–8792.
11. Kwon, K. W., H. Park, …, J. Doh. 2012. Nanotopography-guided migration of T cells. *J. Immunol.* 189:2266–2273.
12. Kumar, G., C.-C. Ho, and C. C. Co. 2007. Guiding cell migration using one-way micropattern arrays. *Adv. Mater.* 19:1084–1090.
13. Mahmud, G., C. J. Campbell, …, B. A. Grzybowski. 2009. Directing cell motions on micropatterned ratchets. *Nat. Phys.* 5:606–612.
14. Kushiro, K., S. Chang, and A. R. Asthagiri. 2010. Reprogramming directional cell motility by tuning micropattern features and cellular signals. *Adv. Mater.* 22:4516–4519.
15. Kumar, G., C. C. Co, and C.-C. Ho. 2011. Steering cell migration using microarray amplification of natural directional persistence. *Langmuir.* 27:3803–3807.
16. Yoon, S.-H., Y. K. Kim, …, M. R. Mofrad. 2012. Passive control of cell locomotion using micropatterns: the effect of micropattern geometry on the migratory behavior of adherent cells. *Lab Chip.* 12:2391–2402.
17. Ko, Y.-G., C. C. Co, and C.-C. Ho. 2013. Directing cell migration in continuous microchannels by topographical amplification of natural directional persistence. *Biomaterials.* 34:353–360.
18. Ko, Y.-G., C. C. Co, and C.-C. Ho. 2013. Gradient-free directional cell migration in continuous microchannels. *Soft Matter.* 9:2467–2474.
19. Smith, J. T., J. K. Tomfohr, …, W. M. Reichert. 2004. Measurement of cell migration on surface-bound fibronectin gradients. *Langmuir.* 20:8279–8286.
20. Lo, C. M., H. B. Wang, …, Y. L. Wang. 2000. Cell movement is guided by the rigidity of the substrate. *Biophys. J.* 79:144–152.
21. Ananthakrishnan, R., and A. Ehrlicher. 2007. The forces behind cell movement. *Int. J. Biol. Sci.* 3:303–317.
22. Feynman, R., R. Leighton, and M. Sands. 1963. The Feynman Lectures on Physics. *In* The Feynman Lectures on Physics Addison-Wesley, Reading, MA, 41–I.
23. Prost, J., J.-F. Chauwin, …, A. Ajdari. 1994. Asymmetric pumping of particles. *Phys. Rev. Lett.* 72:2652–2655.
24. Jülicher, F., A. Ajdari, and J. Prost. 1997. Modeling molecular motors. *Rev. Mod. Phys.* 69:1269–1281.
25. Mills, C. A., J. G. Fernandez, …, J. Samitier. 2008. The use of high glass temperature polymers in the production of transparent, structured surfaces using nanoimprint lithography. *Microelectron. Eng.* 85:1897–1901.
26. Comelles, J., V. Hortigüela, …, E. Martínez. 2012. Versatile gradients of covalently bound proteins on microstructured substrates. *Langmuir.* 28:13688–13697.
27. Caballero, D., R. Voituriez, and D. Riveline. 2014. Protrusion fluctuations direct cell motion. *Biophys. J.* 107:34–42.

28. Le Berre, M., Y.-J. Liu, …, M. Piel. 2013. Geometric friction directs cell migration. *Phys. Rev. Lett.* 111:198101–198106.

29. Smith, J. T., J. T. Elkin, and W. M. Reichert. 2006. Directed cell migration on fibronectin gradients: effect of gradient slope. *Exp. Cell Res.* 312:2424–2432.

30. Selmeczi, D., S. Mosler, …, H. Flyvbjerg. 2005. Cell motility as persistent random motion: theories from experiments. *Biophys. J.* 89:912–931.

31. Selmeczi, D., L. Li, …, H. Flyvberg. 2008. Cell motility as random motion: A review. *Eur. Phys. J. Spec. Top.* 157:1–15.

32. Constantini, G., and F. Marchesoni. 1999. Threshold diffusion in a tilted washboard potential. *Europhys. Lett.* 48:491–497.

33. Khatau, S. B., C. M. Hale, …, D. Wirtz. 2009. A perinuclear actin cap regulates nuclear shape. *Proc. Natl. Acad. Sci. USA.* 106:19017–19022.

34. Pajerowski, J. D., K. N. Dahl, …, D. E. Discher. 2007. Physical plasticity of the nucleus in stem cell differentiation. *Proc. Natl. Acad. Sci. USA.* 104:15619–15624.

35. Ghibaudo, M., L. Trichet, …, B. Ladoux. 2009. Substrate topography induces a crossover from 2D to 3D behavior in fibroblast migration. *Biophys. J.* 97:357–368.

36. Wolf, K., M. Te Lindert, …, P. Friedl. 2013. Physical limits of cell migration: control by ECM space and nuclear deformation and tuning by proteolysis and traction force. *J. Cell Biol.* 201:1069–1084.

37. Mak, M., C. A. Reinhart-King, and D. Erickson. 2013. Elucidating mechanical transition effects of invading cancer cells with a subnucleus-scaled microfluidic serial dimensional modulation device. *Lab Chip.* 13:340–348.

38. Tranquillo, R. T., D. A. Lauffenburger, and S. H. Zigmond. 1988. A stochastic model for leukocyte random motility and chemotaxis based on receptor binding fluctuations. *J. Cell Biol.* 106:303–309.

39. Harris, T. H., E. J. Banigan, …, C. A. Hunter. 2012. Generalized Lévy walks and the role of chemokines in migration of effector CD8+ T cells. *Nature.* 486:545–548.

40. Hughes, B. D. 1995. Random Walks and Random Environments: Random Walks. Oxford University Press.